Aerospace Science and Technology 66 (2017) 103–111

Contents lists available at ScienceDirect

Aerospace Science and Technology

www.elsevier.com/locate/aescte

A robust predictor–corrector entry guidance

Wang Tao, Zhang Hongbo *, Zeng Liang, Tang Guojian

College of Aerospace Science and Engineering, National University of Defense Technology, Changsha 410073, China

ARTICLE INFO

Article history:
Received 6 August 2016
Received in revised form 10 February 2017
Accepted 6 March 2017
Available online 10 March 2017

Keywords:
Entry
Guidance
Predictor–corrector
Fuzzy logic
Drag acceleration

ABSTRACT

With the development of aerospace industry, the guidance system of an entry vehicle becomes more robust, reliable and autonomous. Based on fuzzy logic, a predictor–corrector guidance law is proposed in this paper, where the trajectory prediction is realized by numerical integration. The correction system consists of two fuzzy controllers, which correct longitudinal motion and lateral motion synergistically. A drag acceleration profile is designed through interpolating between upper drag boundary and lower drag boundary, which is corrected continually to eliminate the range error. Attack angle, a secondary control variable in the paper, is used to eliminate the altitude error. In addition, the lateral error is removed by regulating the reversal time of bank angle. Compared with the traditional guidance laws, the method in this paper not only can correct synergistically the longitudinal motion and lateral motion of the vehicle, but also can easily cope with the flight constraints using interpolated drag acceleration profile. Moreover, in a correction cycle, the method designed in this paper only needs a single trajectory prediction, which reduces the on-board computation. The guidance law demonstrates a high precision and robustness in the simulation scenario.

1. Introduction

The research on lifting entry guidance has experienced two stages. The first stage started in the 1970s. The main study was aimed at the entry of shuttle plane and the classical guidance law based on drag acceleration profile was shaped [1]. The second development upsurge arose in the 90s of the last century. With the development of the new generation RLV, NASA started the research for advanced guidance and control systems. During that period, many guidance methods have been proposed. The remarkable achievements are the Evolved Acceleration Guidance Logic for Entry (EAGLE), proposed by Mease [2,3], and the guidance law based on Quasi-Equilibrium Glide Condition (QEGC), advocated by Lu [4]. In recent years, the study of entry guidance has entered a new era. The robustness, reliability and autonomy of entry guidance systems are increasingly gaining attention.

The entry guidance methods can be divided into two categories: trajectory planning–tracking guidance methods and predictor–corrector guidance methods. The first class has been successfully used in shuttle plane, whereas it closely depends on a reference trajectory. The other class includes trajectory prediction and command correction. Because the guidance commands are continually corrected based on the prediction results, these methods exhibit a better performance in robustness and flexibility. However, they can hardly be used in engineering due to large amounts of computation.

The research on predictor–corrector guidance can date back to the 80s of the last century, which was started in the exploration of Mars. Because of the limited capacity of computing, the analytical way of trajectory prediction is developed. Due to some simplifications within the procedure, the prediction precision is low [5,6]. With the development of computer technology, researchers gradually turn to the numerical way of prediction. In 1970s, Powell designed a predictor–corrector guidance law for rescue spacecraft and Mars probe [7]. The Runge–Kutta numerical integration was used to predict trajectory and the dichotomy was used to correct roll angle. Xue [8] and Li [9] transform flight constraints into the limits of bank angle based on QEGC, and use Newton–Raphson iteration to correct the linear bank angle profile. The bank angle reversal is determined by a cross-range function or an azimuth error band. Yong [10] uses some waypoints to divide the flight trajectory into several subsections. In each subsection, the state at the next waypoint, instead of the terminal state, is predicted, which reduces the prediction time. But a reference trajectory is necessary which restricts the feasibility of the method. Xu [11] uses BP network to predict flight trajectory, in which a great amount of flight data is required to train the network. Lu [12] extends the results in Reference [8], and proposes a universal guidance method for vehicles with both high lift-to-drag ratio and low high lift-to-drag ratio. Moreover, a Fully Numerical Entry Guidance Algorithm (FNEGA) is

* Corresponding author.
E-mail address: zhanghb1304@nudt.edu.cn (H. Zhang).

http://dx.doi.org/10.1016/j.ast.2017.03.010
1270-9638/

proposed by Lu [13], which can be applied to both direct entry and skip entry, regardless of the lift-to-drag ratio of vehicle. However, the lateral guidance still uses a cross-range function in FNEGA.

In this paper, we develop a predictor–corrector guidance method based on fuzzy logic. The entry course is divided into two phases, initial phase and glide phase. The initial phase is guided by a constant bank angle, which is determined by the errors of initial flight state, atmospheric density and aerodynamic coefficients. In the glide phase, flight trajectory is predicted by Runge–Kutta numerical integration. Two fuzzy controllers are designed to guide the 3-dimensional motion of the vehicle. The longitudinal motion is guided by adjusting the drag acceleration and attack angle. The lateral errors are eliminated by adjusting the reversal time of bank angle. Considering the longitudinal motion and lateral motion are corrected synergistically, the predictor–corrector guidance method improves the robustness and flexibility of entry motion. In view of the fact that the drag acceleration profile is obtained by interpolating between the upper and lower boundaries of flight corridor, the flight constraints can be easily dealt with. Moreover, the traditional correction strategy is improved. Only a single trajectory prediction is needed in a guidance cycle, which is favorable for on-board computation.

2. Basic model

2.1. Dynamic equations

The dynamic equations of entry vehicle are given by

$$\begin{cases} \dfrac{\mathrm{d}r}{\mathrm{d}t} = V\sin\theta \\ \dfrac{\mathrm{d}\lambda}{\mathrm{d}t} = \dfrac{V\cos\theta\sin\psi}{r\cos\phi} \\ \dfrac{\mathrm{d}\phi}{\mathrm{d}t} = \dfrac{V\cos\theta\cos\psi}{r} \\ \dfrac{\mathrm{d}V}{\mathrm{d}t} = -D - g\sin\theta + C_V \\ \dfrac{\mathrm{d}\theta}{\mathrm{d}t} = \dfrac{L\cos\sigma}{V} - \dfrac{g\cos\theta}{V} + \dfrac{V\cos\theta}{r} + C_\theta \\ \dfrac{\mathrm{d}\psi}{\mathrm{d}t} = \dfrac{L\sin\sigma}{V\cos\theta} + \dfrac{V\tan\phi\cos\theta\sin\psi}{r} + C_\psi \end{cases} \tag{1}$$

where r is the radial distance from the center of the Earth to the vehicle, V is the velocity of the vehicle, λ is the longitude, ϕ is the latitude, θ is the flight path angle, and ψ is the heading angle. In addition, σ is the bank angle, g is the gravitational acceleration, L and D represent the lift and drag accelerations, respectively. C_V, C_θ and C_ψ account for the contribution of Coriolis acceleration and convected acceleration.

$$\begin{cases} C_\psi = 2\omega_e(\sin\phi - \cos\psi\tan\theta\cos\phi) \\ \qquad + \dfrac{\omega_e^2 r\cos\phi\sin\phi\sin\psi}{V\cos\theta} \\ C_\theta = 2\omega_e\sin\psi\cos\phi \\ \qquad + \dfrac{\omega_e^2 r}{V}\cos\phi(\sin\phi\cos\psi\sin\theta + \cos\phi\cos\theta) \\ C_V = \omega_e^2 r\left(\cos^2\phi\sin\theta - \cos\phi\sin\phi\cos\psi\cos\theta\right) \end{cases} \tag{2}$$

where ω_e is the self-rotation rate of the Earth. For simplification, the dynamic equations are transformed into the P coordinate system [14].

In Fig. 1, N is the north pole of the Earth. The longitude and latitude of the entry point (I) are denoted by (λ_0, ϕ_0). A_0 is the angle between meridian plane and the plane determined by entry point and target point T (the reference plane). The P coordinate system is described as follows: X_P is aligned in the direction of the initial radial vector, and Y_P is perpendicular to X_P in the reference plane. X_P, Y_P, and Z_P constitute a right-hand coordinate system. P is on the Z_P axis, and denotes the "north pole" of the P coordinate system. PNI is a spherical triangle, whose arc PI is $\pi/2$ rad.

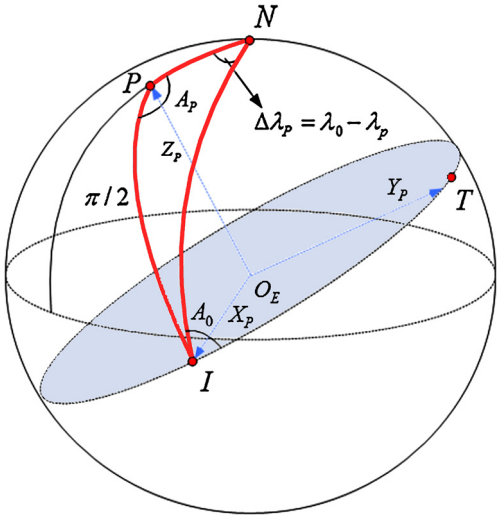

Fig. 1. P coordinate system.

In the P coordinate system, λ_0 and ϕ_0 are set as zeros. The reference plane is the zero-latitude plane. The latitude denotes the lateral deviation of the vehicle. The variables in the rest of this paper are in the P coordinate system.

2.2. Constraints

In the flight, the constraints on heating rate, aerodynamic load, and dynamic pressure should be considered. In the traditional guidance method, a drag acceleration corridor is built based on those constraints. Within the corridor, a drag acceleration profile is designed to guide the vehicle. The lower boundary of the corridor is determined by QEGC.

$$D_{\mathrm{QEGC}} = \frac{(g - V^2/r) + K}{C_L/C_D\cos\sigma} \tag{3}$$

where K is the self-rotation effect of the Earth. C_L and C_D are respectively the lift and drag coefficients. The upper boundary of the corridor is determined by the maximum heating rate $Q_{\max}$, maximum aerodynamic load $q_{\max}$, and maximum dynamic pressure $n_{\max}$.

$$\begin{cases} D \le D_Q = \dfrac{C_D S_r Q_{\max}^2}{2Mk_Q^2 V^{2m-2}} \\ D \le D_q = \dfrac{q_{\max} C_D S_r}{M} \\ D \le D_n = \dfrac{n_{\max} g_0}{\sqrt{1 + (C_L/C_D)^2}} \end{cases} \tag{4}$$

where, S_r is the reference area of the vehicle, M is the mass of the vehicle, $m = 3.15$ and k_Q is the parameter of heating model.

To meet the requirement of Terminal Area Energy Management (TAEM), the terminal states of the entry course are limited by

$$\begin{cases} r_f = r_{TAEM} \\ V_f = V_{TAEM} \\ S_{togo,f} = R_{TAEM} \\ \Delta\psi_f \le \varepsilon \end{cases} \tag{5}$$

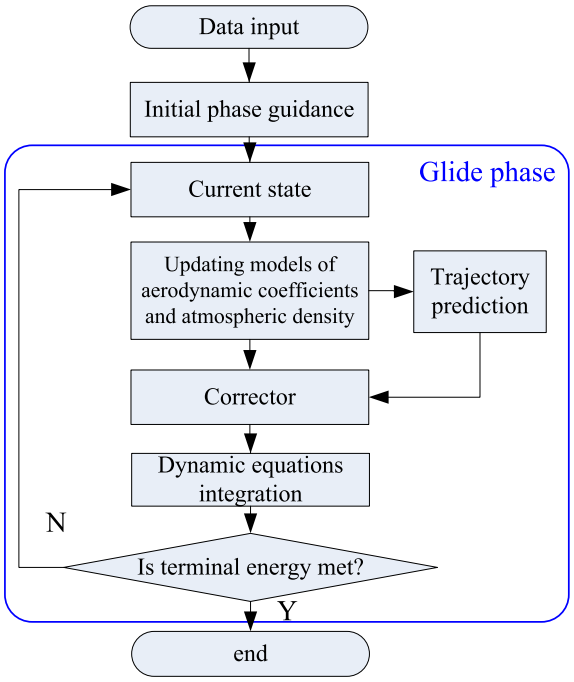

Fig. 2. Research framework.

where, $S_{togo,f}$ is the terminal range-to-go and R_{TAEM} is the radius of TAEM. $\Delta\psi_f$ is the difference between the terminal heading angle and the line-of-sight angle, ε is a small positive constant.

The control variables are bank angle and attack angle, in which the bank angle plays a major role.

$$\begin{aligned} &\alpha \in [\alpha_{\min}, \alpha_{\max}], \quad |\mathrm{d}\alpha/\mathrm{d}t| \le |\mathrm{d}\alpha/\mathrm{d}t|_{\max} \\ &\sigma \in [\sigma_{\min}, \sigma_{\max}], \quad |\mathrm{d}\sigma/\mathrm{d}t| \le |\mathrm{d}\sigma/\mathrm{d}t|_{\max} \end{aligned} \tag{6}$$

In the entry course, $\alpha_{\min}$ is designed as the attack angle of the maximum lift-drag ratio. $\sigma_{\min}$ and $\sigma_{\max}$ are determined by the constraints on heating rate, aerodynamic load and dynamic pressure. $\alpha_{\max}$, $|\mathrm{d}\alpha/\mathrm{d}t|_{\max}$ and $|\mathrm{d}\sigma/\mathrm{d}t|_{\max}$ are determined by the structure of the vehicle.

3. Entry guidance

The entry course is divided into two phases, initial phase and glide phase. The research framework of this paper is shown as Fig. 2.

The guidance law of the initial phase is designed to be simple, because of the thin atmosphere and the non-QEGC flight. In the glide phase, the errors of aerodynamic coefficients and atmospheric density are identified first, which is very important for trajectory prediction. The trajectory prediction is realized by numerical integration. The prediction results are delivered to the corrector, which is based on fuzzy controller. The corrector generates guidance commands, which are then delivered to the model of the vehicle.

3.1. Initial phase

In the initial phase, a constant bank angle is designed to guide the vehicle. To make the entry more flexible, the value of the bank angle is regulated based on state errors and model errors. Through analysis, the errors of initial velocity, initial flight path angle, aerodynamic coefficients and atmospheric density have a greater influence on entry course. So, the bank angle of the initial phase is designed as

$$|\sigma_{ini}| = |\sigma_{ini}|_0 + a\Delta(L/D) + b\Delta\rho + c\Delta\theta_0 + d\Delta V_0 \tag{7}$$

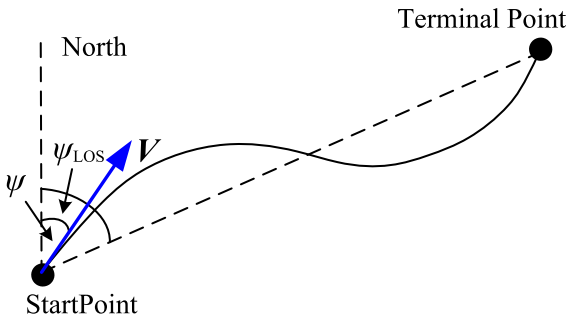

Fig. 3. Heading angle and line-of-sight angle.

where $|\sigma_{ini}|_0$ is the bank angle without considering errors. $\Delta(L/D)$ is the error of lift-to-drag ratio, $\Delta\rho$ is the error of atmospheric density, $\Delta\theta_0$ is the error of initial flight path angle, and ΔV is the error of initial velocity. $\Delta\rho$ is identified based on indirect measurement and standard atmospheric density model. a, b, c and d are determined through simulation analysis, which should keep the heating rate within constraint.

The sign of the bank angle is determined by the initial heading angle and the line-of-sight angle.

$$\mathrm{sign}(\sigma_{ini}) = -\mathrm{sign}(\psi - \psi_{\mathrm{LOS}}) \tag{8}$$

where ψ_{LOS} is the line-of-sight angle, as shown in Fig. 3.

The transition point between initial phase and glide phase is determined by

$$\left|\mathrm{d}r/\mathrm{d}V - (\mathrm{d}r/\mathrm{d}V)_{\mathrm{QEGC}}\right| < \delta \tag{9}$$

where $\mathrm{d}r/\mathrm{d}V = -V\sin\theta/(D + g\sin\theta)$. $(\mathrm{d}r/\mathrm{d}V)_{\mathrm{QEGC}}$ is the slope of QEGC at the current point $(r,\ V)$, and it can be obtained by differentiating the QEGC with respect to V. δ is a small positive scalar.

The bank angle of the transition point is obtained by QEGC, which guarantees no skip on height in the beginning of the glide phase.

$$|\sigma_{tran}| = \arccos\frac{g - V^2/r + K}{L} \tag{10}$$

3.2. Trajectory prediction

The predictor is based on Runge–Kutta numerical integration. In the dynamic prediction model, energy is chosen as the independent variable, rather than time. To integrate these differential equations, the attack angle model and the bank angle model should be designed. When the energy of the vehicle meets the terminal requirement, the integration ends. Taking the unmanned Lockheed Martin X-33 space plane as research object, the attack angle profile is

$$\alpha = \begin{cases} \alpha_0 & \text{if } Ma \ge 10 \\ \alpha_0 - \dfrac{(\alpha_0 - \alpha_f)}{(Ma_f - 10)^2}(Ma - 10)^2 & \text{if } 3 \le Ma \le 10 \end{cases} \tag{11}$$

where α_0 is designed to be a large value, such as 45°, which is beneficial to reducing heating rate. α_f needs to be set at around the attack angle of maximum lift-drag ratio, $\alpha_{\max L/D}$, considering the attack angle of TAEM is almost below $\alpha_{\max L/D}$.

Instead of the bank angle, the drag acceleration, an indirect control variable, is designed to predict the entry trajectory. The drag acceleration profile is shown in Fig. 4. The corridor is determined by equation (3) and equations (4). Because the upper boundary is composed of three segments, its differential is discontinuous. So the modified upper boundary, D_{maxF}, is designed as follows

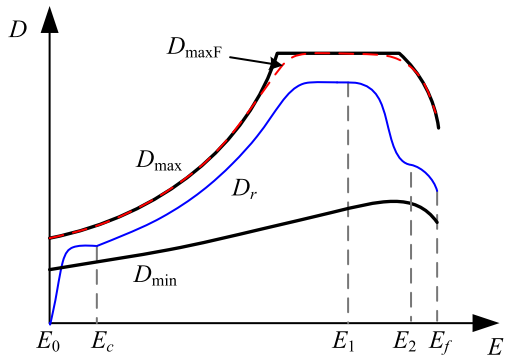

Fig. 4. Drag acceleration profile.

$$D_{\mathrm{maxF}} = \begin{cases} D_{\max} & \text{if } E < 0.55 \text{ or } E > 0.7 \\ a_2E^3 + b_2E^2 + c_2E + d_2 & \text{else} \end{cases} \tag{12}$$

where E is the dimensionless energy of the vehicle. a_2, b_2, c_2, and d_2 are determined by the $D_{\max}$ of $E = 0.55$ and $E = 0.7$ and their differentials. The differential of $D_{\max}$ with respect to E is

$$\begin{cases} \dfrac{\mathrm{d}D_{\max,\dot{Q}}}{\mathrm{d}E} = \dfrac{S_r\dot{Q}_{\max}^2}{2Mk_Q^2}\left(\dfrac{V\dot{C}_D - (2m-2)C_D(\mathrm{d}V/\mathrm{d}E)}{V^{2m-3}}\right) \\ \dfrac{\mathrm{d}D_{\max,q}}{\mathrm{d}E} = \dfrac{q_{\max}S_r(\mathrm{d}C_D/\mathrm{d}E)}{M} \\ \dfrac{\mathrm{d}D_{\max,n}}{\mathrm{d}E} = \dfrac{-n_{\max}g_0C_L/C_D}{(1+(C_L/C_D)^2)^{1.5}} \cdot \dfrac{C_D(\mathrm{d}C_L/\mathrm{d}E) - C_L(\mathrm{d}C_D/\mathrm{d}E)}{C_D^2} \end{cases} \tag{13}$$

where $\mathrm{d}V/\mathrm{d}E$, $\mathrm{d}C_D/\mathrm{d}E$ and $\mathrm{d}C_L/\mathrm{d}E$ are respectively the differentials of V, C_D and C_L with respect to E. Considering $\mathrm{d}V/\mathrm{d}E \approx 1/V$, it is easy to calculate the right side of Equations (13).

When D_{maxF} is obtained, the reference profile of D is designed as the interpolation between upper drag boundary and lower drag boundary.

$$D_{std} = D_{\min} + k_d(D_{\mathrm{maxF}} - D_{\min}) \tag{14}$$

where k_d is the scale factor. Since $k_d \in [0, 0.98]$, the drag acceleration can be safely kept within the corridor. The initial value of k_d is determined by the initial state of the vehicle. When the terminal state is constrained and the attack angle model has been planned, the terminal value of k_d is also determined. Then, k_d can be designed as

$$k_d = \begin{cases} k_{dc}, & E \le E_1 \\ k_{dc} + \dfrac{k_{df} - k_{dc}}{E_2 - E_1}(E - E_1), & E_1 < E \le E_2 \\ k_{df}, & E \ge E_2 \end{cases} \tag{15}$$

where, k_{dc} is the current value of k_d. k_{df} is the terminal value of k_{df}. E_1 and E_2 are designed nodes. Equation (14) and equation (15) describe the reference profile of D, as shown in Fig. 4.

The bank angle can be obtained from drag acceleration.

$$\frac{L}{D}\cos\sigma = a_d\left(\frac{\mathrm{d}^2D}{\mathrm{d}E^2} - b_d\right) \tag{16}$$

where

$$a_d = -h_sV^2$$

$$b_d = D\left(\frac{1}{C_D}\frac{\mathrm{d}^2C_D}{\mathrm{d}E^2} - \frac{1}{C_D^2}\left(\frac{\mathrm{d}C_D}{\mathrm{d}E}\right)^2\right) + \frac{\mathrm{d}D}{\mathrm{d}E}\left(\frac{2}{V^2} + \frac{1}{C_D}\frac{\mathrm{d}C_D}{\mathrm{d}E}\right) - \frac{4D}{V^4} + \left(g - \frac{V^2}{r}\right)\frac{1}{h_sV^2D} - \frac{C_\theta}{h_sVD}$$

where h_s is scale height. $\mathrm{d}^2D/\mathrm{d}E^2$ and $\mathrm{d}^2C_D/\mathrm{d}E^2$ are respectively the second order differential of D and C_D with respect to E.

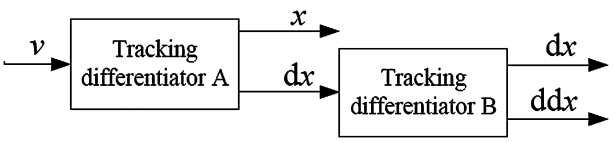

Fig. 5. Serial tracking differentiators.

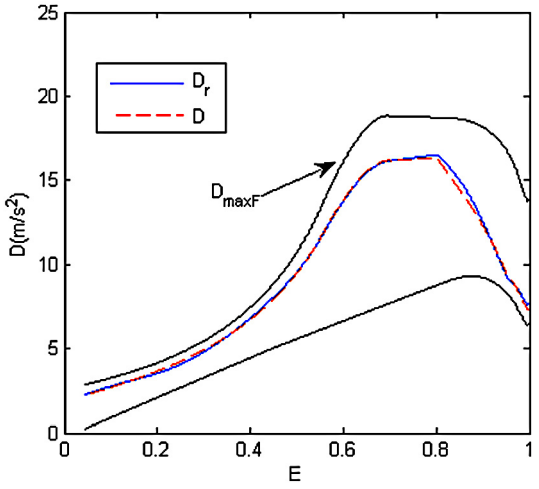

Fig. 6. Drag acceleration profile in prediction.

The differentials of equation (16) are obtained by tracking differentiator (TD), which has a better performance in differential calculation. The application of TD is shown in Fig. 5.

In Fig. 5, v is the input signal. x is the track of v and $\mathrm{d}x$ is the differential of v. The expression of TD is

$$\begin{cases} x^{k+1} = x^k + h \cdot \mathrm{d}x^k \\ \mathrm{d}x^{k+1} = \mathrm{d}x^k + h \cdot FH \end{cases} \quad k = 1, 2, 3\ldots \tag{17}$$

where, h is the step size of numerical integration. k denotes the k-th step. FH is the output of a nonlinear function.

$$FH = fhan(x_1, x_2, \gamma, h_0) \tag{18}$$

where, $x_1 = x^k - v^k$, $x_2 = \mathrm{d}x^k$, γ is a constant. The larger the value of γ is, the faster the track. $h_0 = ch$, $c \in Z^+$, is served as a low pass filter. The expression of $fhan$ is

$$\begin{cases} d = rh_0^2 \\ a_0 = h_0x_2 \\ y = x_1 + a_0 \\ a_1 = \sqrt{d(d + 8|y|)} \\ a_2 = a_0 + sign(y)(a_1 - d)/2 \\ a = (a_0 + y)fsg(y, d) + a_2\big(1 - fsg(y, d)\big) \\ fhan = -r(a/d)fsg(a, d) - rsign(a)\big(1 - fsg(a, d)\big) \end{cases} \tag{19}$$

where, fsg is defined as

$$fsg(\xi, d) = \big(sign(\xi + d) - sign(\xi - d)\big)/2 \tag{20}$$

To integrate the dynamic equations, the sign of bank angle is also needed to be determined. Through analysis, two reversals of bank angle can meet the requirement of entry course and guarantee a better motion characteristic. The reversal times are adjusted by the command corrector until the lateral error is zero.

Based on the serial TDs, the real drag acceleration in trajectory prediction is generated, as shown in Fig. 6.

In the trajectory prediction, the terminal position is continually adjusted based on the heading angle of the vehicle, which can

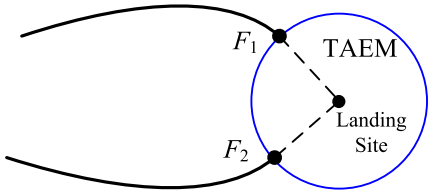

Fig. 7. Determination of terminal point.

make the vehicle entry TAEM vertically. For example, in Fig. 7, the terminal positions of two trajectories are different.

The terminal position is calculated as follows.

$$\begin{cases} \lambda_f = \lambda_T - \cos(\psi - 0.5\pi) R_{\text{TAEM}}/r \\ \phi_f = \phi_T - \sin(\psi - 0.5\pi) R_{\text{TAEM}}/r \end{cases} \tag{21}$$

where λ_T and ϕ_T denote the longitude and the latitude of landing site respectively.

3.3. Command corrector

In traditional correction methods, researchers try to find an accurate bank angle through iteration. However, the iteration needs several times of trajectory predictions, which is difficult to implement on-board in an acceptable time. When the iteration is finished, the bank angle, obtained based on the data before iteration, is not accurate any more. What is worse, when considering the effect of bank angle reversal and the non-spherical perturbation of the Earth, the monotony relationship between bank angle and flight range may not be true. In that case, the effect of Newton–Raphson iteration may not be acceptable. So, in this paper, we use fuzzy controller to correct the guidance commands. Only once trajectory prediction is required in a single correction cycle, which reduces time consumption largely. Although the method cannot offer a very accurate command in once correction, the terminal error gradually converges to zero as the system evolves.

3.3.1. Correction of the drag acceleration profile

Range-to-go is an important parameter in longitudinal guidance. Its differential equation is $\mathrm{d}R_{togo}/\mathrm{d}t = -V\cos\theta\cos\Delta\psi/r$, where $\Delta\psi$ is assumed to be zero or a small constant. Based on this equation, an analytical expression of range-to-go is deduced in the guidance of shuttle. In the traditional predictor–corrector guidance method, that differential equation is also used to predict the range-to-go. The first, the fourth, and the fifth equation of equations (1) constitute the reduced longitudinal dynamic equations. Using the reduced dynamic equations for prediction, the prediction speed is improved a little. However, those methods assume that the entry trajectory is a great circle arc. The lateral maneuver is not considered. So, to improve the prediction precision we use the full dynamic models to predict the trajectory. The flight range R is the arc between the initial point and the predicted terminal point.

$$\Delta R = R - R_0 \tag{22}$$

where R_0 is the arc between the initial point and the nominal terminal point, and ΔR is the range error.

The fuzzy controller 1 (FC1) is designed to correct the parameter of the D profile, k_{dc}. The input variables of FC1 are ΔR and R_{togo}. The fuzzification of the input variables are shown in Fig. 8 and Fig. 9. The output variable of FC1 is the delta of k_d. The defuzzification of the output variable is shown in Fig. 10. The rules of FC1 are shown in Table 1, which build relationships between the input and the output of the controller.

The fuzzy controller is designed based on the analysis of entry motion.

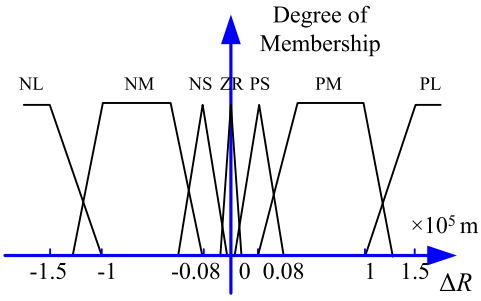

Fig. 8. Membership function of range error.

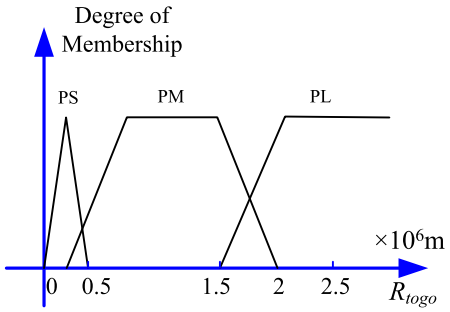

Fig. 9. Membership function of range-to-go.

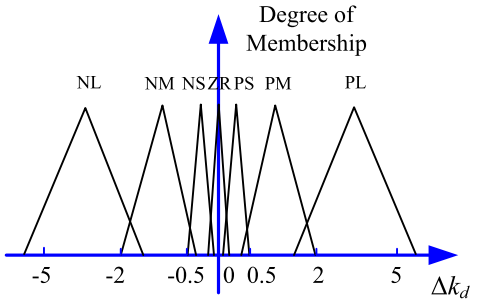

Fig. 10. Membership function of Δk_d.

Table 1
Rules for bank angle.

R_{togo} \ ΔR	NL	NM	NS	ZR	PS	PM	PL
PS	NL	NL	NM	ZR	PM	PL	PL
PM	NL	NM	NS	ZR	PS	PM	PL
PL	NL	NM	NS	ZR	PS	PM	PL

The inputs: the flight range is partitioned with 7 membership functions, {NL, NM, NS, ZR, PS, PM, PL}. The domains of NS, ZR and PS should be small, which helps to improve the sensitivity of fuzzy controller.

The outputs: the outputs are preliminarily partitioned with equal membership functions.

Fuzzy rules: the fuzzy rules are built based on the logical relationship (qualitative analysis) between control variables and flight range.

Fuzzy Logic Toolbox of Matlab software is used to picture the relationship between inputs and outputs. If the relationship is not satisfactory, the membership functions and fuzzy rules are modified. For different mission, it is not necessary to design a new fuzzy controller. Through adjusting η_c of equation (18), we can get an acceptable guidance effect.

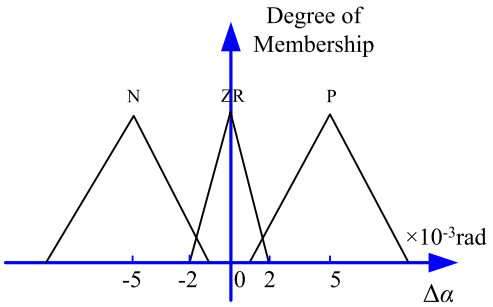

Fig. 11. Membership function of $\Delta\alpha$.

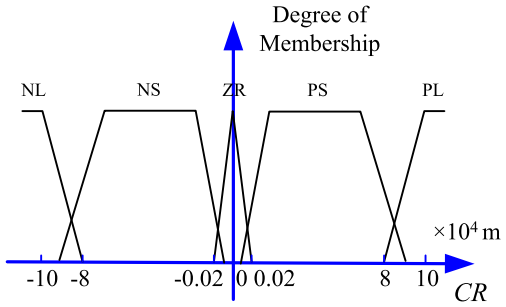

Fig. 12. Membership function of cross-range.

Table 2
Rules for attack angle.

ΔR / R_{togo}	NL	NM	NS	ZR	PS	PM	PL
PS	ZR	ZR	ZR	ZR	ZR	ZR	ZR
PM	N	ZR	ZR	ZR	ZR	ZR	P
PL	N	ZR	ZR	ZR	ZR	ZR	P

After Δk_d is obtained, the current k_{dc} is corrected as

$$\begin{cases} k'_{dc} = k_{dc,pre} + \Delta k_d \\ k_{dc} = \eta_c k'_{dc} + (1-\eta_c) k_{dc,pre} \end{cases} \tag{23}$$

where $\eta_c \in [0,1]$, which avoids the drastic change of the bank angle. $k_{dc,pre}$ is the value of k_{dc} of the last correction cycle. For different missions, it is not necessary to alter the fuzzy controller. Through adjusting η_c we can obtain an acceptable guidance performance.

When k_{dc} is obtained, we can use equation (14) to calculate the reference drag acceleration. Then a control law is designed to track the reference drag acceleration.

$$\left(\frac{\mathrm{d}^2 D_r}{\mathrm{d}E^2} - \frac{\mathrm{d}^2 D}{\mathrm{d}E^2}\right) + 2\zeta\omega_n\left(\frac{\mathrm{d}D_r}{\mathrm{d}E} - \frac{\mathrm{d}D}{\mathrm{d}E}\right) + \omega_n^2 (D_r - D) = 0 \tag{24}$$

where, ζ is damping ratio and ω_n is natural frequency. D_r is the reference drag acceleration. $\mathrm{d}D_r/\mathrm{d}E$ and $\mathrm{d}^2 D_r/\mathrm{d}E^2$ are obtained by the serial TDs in Fig. 5. $\mathrm{d}D/\mathrm{d}E = -DV\sin\theta/h - 2D^2/V$.

From equation (24) and equation (16), we can eliminate $\mathrm{d}^2 D/\mathrm{d}E^2$ and get the bank angle law.

3.3.2. Correction of attack angle

When the attack angle profile is fixed, the maneuver ability of the vehicle is constrained as well. For some mission that is easy to accomplish, only correcting the bank angle is sufficient, while for some arduous mission, it is necessary to correct both the bank angle and the attack angle. The correction of the attack angle is

$$\alpha_0 = \alpha_{0,pre} + \Delta\alpha \tag{25}$$

where $\alpha_{0,pre}$ is the value of α_0 of the last correction cycle. $\Delta\alpha$ is the other output variable of FC1. The defuzzification of $\Delta\alpha$ is shown in Fig. 11. The rules for attack angle are shown in Table 2.

It can be seen from Table 2 that when R_{togo} is short, the attack angle will not be corrected any more. Then, we can adjust the attack angle to meet the requirement of terminal height.

$$\alpha_f = \alpha_{f,pre} + k_h(h - h_0) \tag{26}$$

where $\alpha_{f,pre}$ is the value of α_f of the last correction cycle.

3.3.3. Correction of the reversal times of bank angle

Two reversals of the bank angle are designed to eliminate the lateral error. The reversal times are continually corrected by fuzzy controller 2 (FC2) until the lateral error is zero. The input of FC2 is cross-range. In the P coordinate system, the cross-range can be expressed as

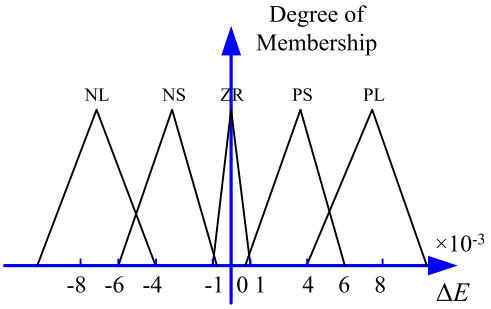

Fig. 13. Membership function of ΔE.

Table 3
Rules of FC2.

L	NL	NS	ZR	PS	PL
ΔE	NL	NS	ZR	PS	PL

$$CR = (\phi_f - \phi_F) \cdot R_E \tag{27}$$

where ϕ_f is the predicted terminal latitude. ϕ_F is the required terminal latitude. R_E is the radius of the Earth. The fuzzification of CR is shown in Fig. 12.

In the paper, the reversal time is defined as the energy of the vehicle where reversal happens. So the output of FC2 is designed as the delta of the energy, ΔE. The defuzzification of ΔE is shown in Fig. 13. The rules of FC2 are shown in Table 3.

When ΔE is obtained, we use equation (28) to determine the reversal time. Because there are two ways of reversal, namely positive-to-negative reversal and negative-to-positive reversal, it is necessary to define the parameter *Sign*.

$$\begin{cases} E'_{rev} = E_{rev,pre} + Sign \cdot \Delta E \\ E_{rev} = \eta_r E'_{rev} + (1-\eta_r) E_{rev,pre} \end{cases} \tag{28}$$

$$Sign = \begin{cases} 1 & sign(\sigma_c) = 1 \\ -1 & sign(\sigma_c) = -1 \end{cases} \tag{29}$$

where $\eta_r \in [0,1]$, which prevents the drastic change of reversal time. E_{rev} is the energy where reversal happens. $E_{rev,pre}$ is the value of E_{rev} of the last correction cycle.

Before the first reversal happens, only the first reversal time is corrected. The second reversal time is fixed until the first reversal is over. To guarantee a favorable heading angle for entry TAEM, the second reversal time needs to be close enough to the terminal point.

Table 4
EG13 mission scenarios.

	h (km)	ϕ (°)	λ (°)	V (m/s)	θ (°)	ψ (°)
Initial state	121.51	−18.26	−117.01	7621.8	−1.44	38.33
Final state	30.43	28.61	−80.14	907.95	−7.5	–

Table 5
Dispersions used in Monte Carlo simulation.

Parameter	h_0 (km)	ϕ_0 (°)	λ_0 (°)	V_0 (m/s)	θ_0 (°)
3σ	±1	±0.5	±0.5	±20	±0.05
Parameter	ψ_0 (°)	Mass_0	C_L	C_D	ρ
3σ	±0.5	±3%	±10%	±10%	±20%

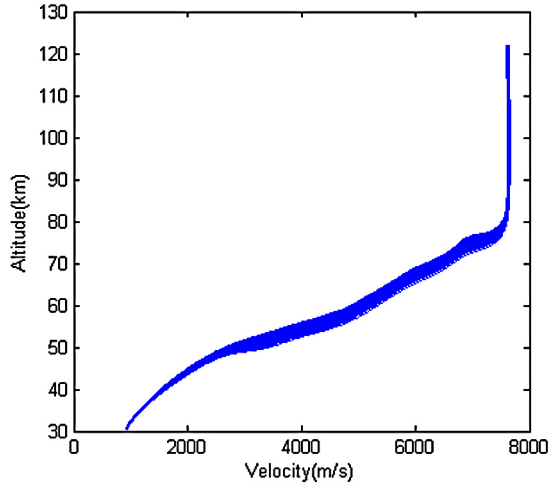

Fig. 14. Velocity–altitude histories.

4. Simulation

To verify the effectiveness of the method proposed in this paper, the EG13 mission of the unmanned Lockheed Martin X-33 space plane is simulated. The mass of X-33 is 37362.9 kg. The applied reference area is 149.388 m^2; the heating rate constraint is 794.425 kW/m^2; the total load constraint is 2.5 g_0; and the dynamic pressure constraint is 14364 Pa. The attack angle rate $|d\alpha/dt|_{max} \leq 5$ deg/s and the bank angle rate $|d\sigma/dt|_{max} \leq 20$ deg/s. The data of the EG13 mission is given in Table 4. The atmosphere model used in simulation is US-1976 standard model. To test the robustness of the guidance, the entry condition, aerodynamic coefficients, atmospheric density and vehicle mass are all dispersed, as shown in Table 5.

At the beginning of the entry, the trajectory prediction takes a long time. The correction cycle needs to be several times of integration cycle, so that in a correction cycle the prediction can be completed. When the prediction time becomes shorter and shorter, the correction can be realized in a single integration cycle. Therefore, large integration step is used in the beginning. When the TAEM is close, small time steps are selected to guarantee a high prediction precision.

Fig. 14 shows 300 velocity–altitude curves of Monte Carlo simulation. In view of the effects of equation (26), when the range-to-go is short, those curves converge to the required terminal state.

Fig. 15 shows the ground trajectories of Monte Carlo simulation. Due to the dispersion of the initial heading angle, the reversal logic of bank angle changes remarkably, which leads to two streams of trajectories. In Fig. 16, the heading angle histories are also divided into two streams. The flight path angle histories in Fig. 17 are all below zero, which indicates that there are no skips in altitude.

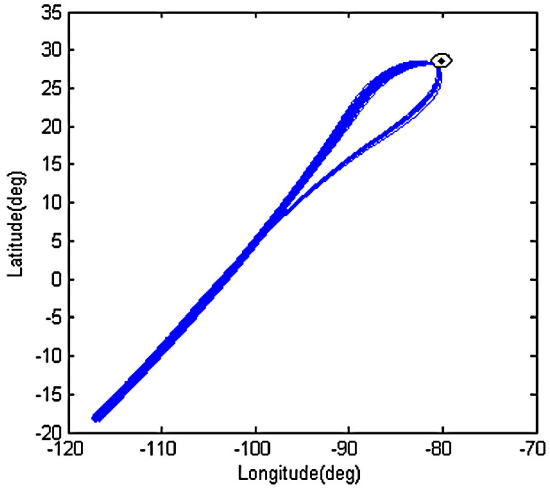

Fig. 15. Ground trajectories.

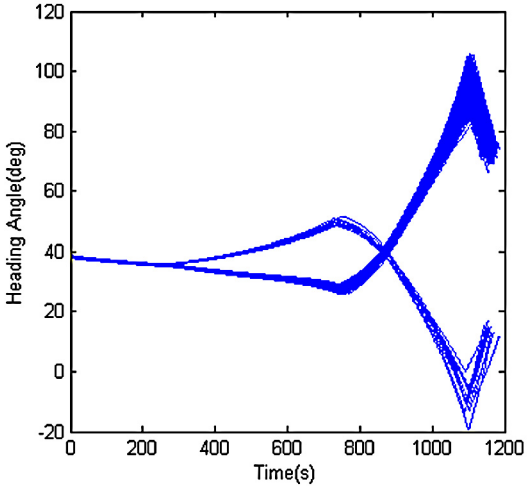

Fig. 16. Heading angle histories.

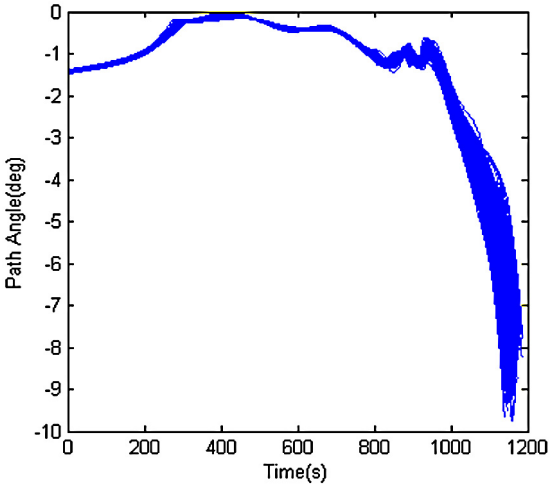

Fig. 17. Flight path angle histories.

Fig. 18 shows the attack angle histories. After the initial phase, the attack angle starts self-adjustment. When the flight range is much longer or shorter than the nominal range, the attack angle will increase or decrease. Fig. 19 shows the bank angle histories. Based on equation (8), the bank angle curves are divided into two

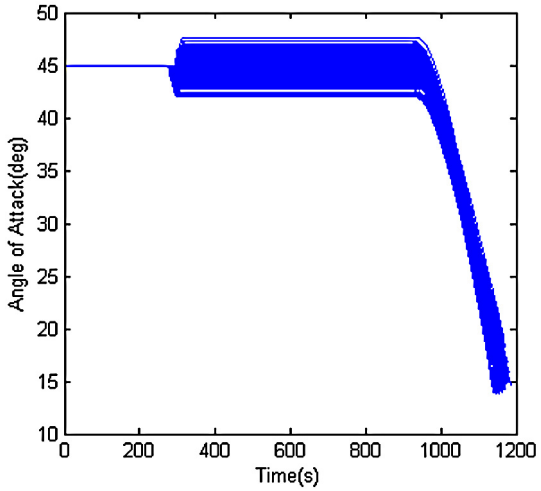

Fig. 18. Attack angle histories.

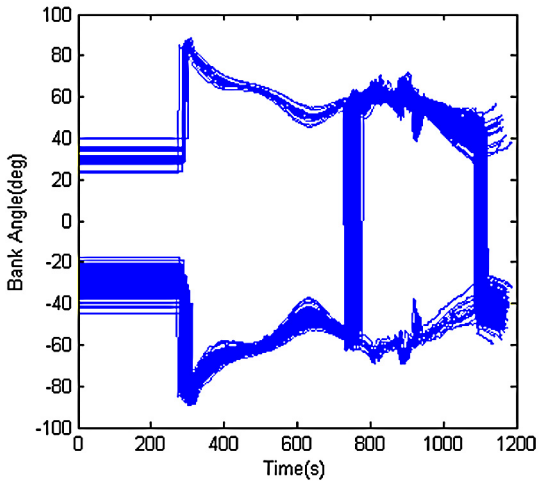

Fig. 19. Bank angle histories.

branches, i.e., a branch with positive initial sign and a branch with negative initial sign. This difference leads to two streams of trajectories in Fig. 15. With the combined control effect of attack angle and bank angle, the vehicle can realize more arduous mission.

Fig. 20, Fig. 21 and Fig. 22 show the histories of heating rate, dynamic pressure and aerodynamic load respectively. Those parameters are within the constraints. At the lowest point of initial phase, the heating rate is easily getting out of range. Using equation (24), the heating rate of this point can be kept within the constraints effectively.

Fig. 23 shows the dispersion of terminal point. Because of the feedback of flight range error, the terminal points almost fall on the TAEM boundary. Fig. 24 and Fig. 25 show the dispersions of terminal velocity and terminal altitude respectively, both of which have a high precision. Although the longitudinal corrector and lateral corrector are designed separately, the proposed guidance method exhibits a good performance. The coupling effect of longitudinal motion and lateral motion can be predicted when it is embodied in the state of the vehicle. Once the coupling is predicted, it can be compensated by the correctors. The correction may produce another coupling effect, but it will be removed in the next guidance cycle.

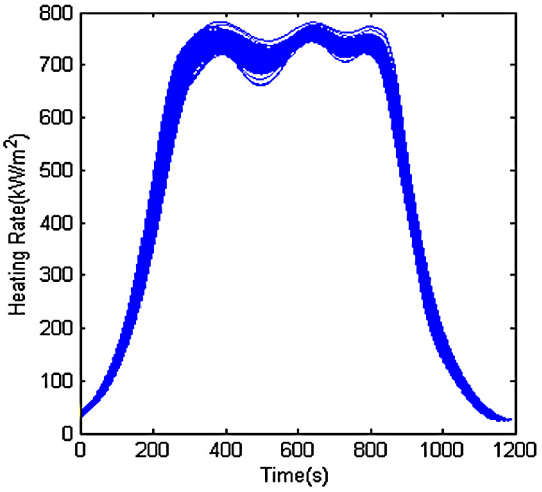

Fig. 20. Heating rate histories.

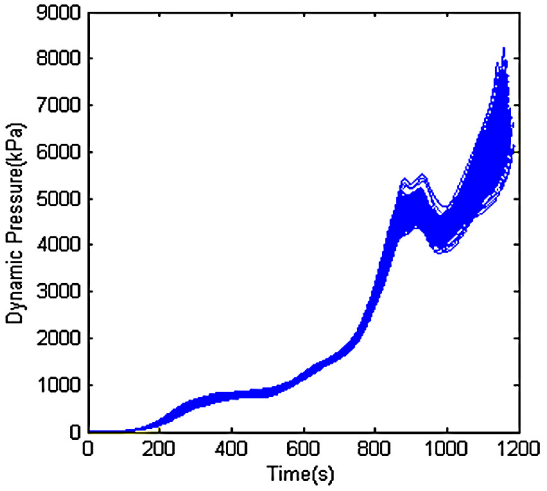

Fig. 21. Dynamic pressure histories.

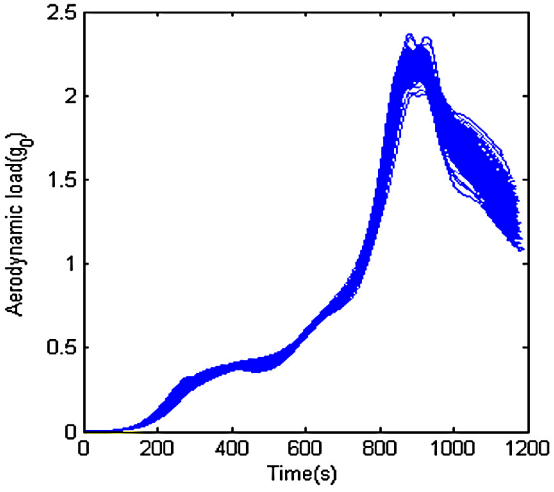

Fig. 22. Aerodynamic load histories.

5. Conclusion

In this paper, we propose a predictor–corrector guidance method based on fuzzy logic. The trajectory prediction is realized by Runge–Kutta numerical integration. The corrector is designed

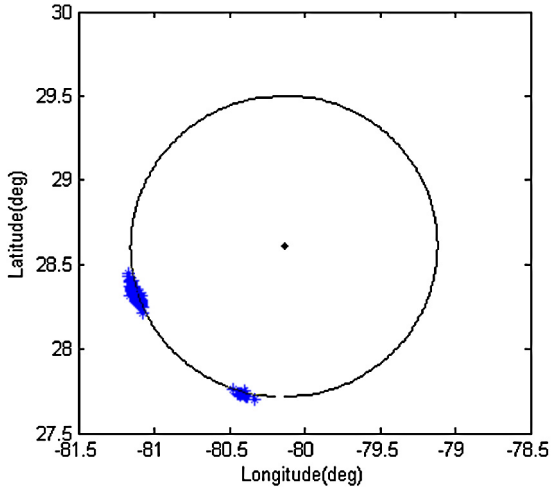

Fig. 23. Dispersion of terminal points.

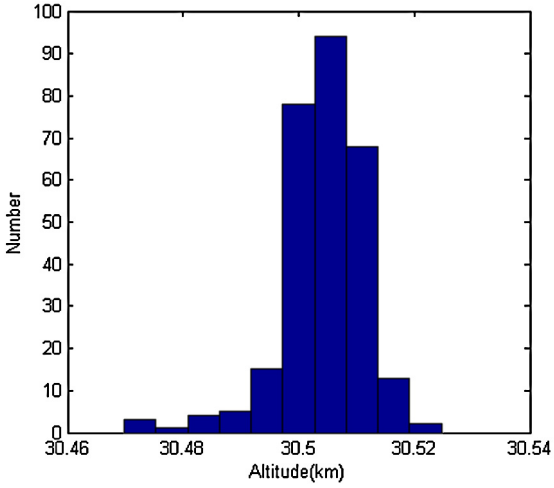

Fig. 24. Dispersion of altitude.

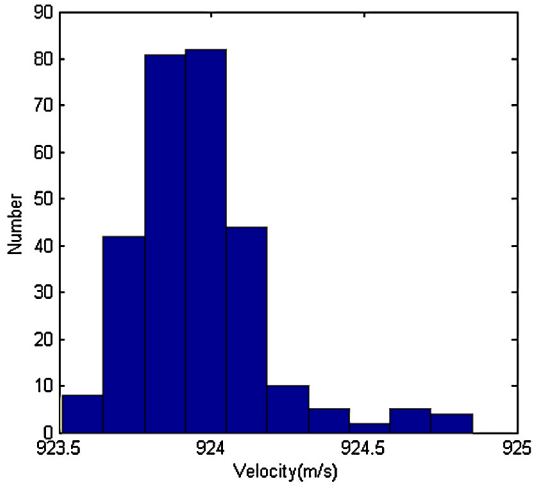

Fig. 25. Dispersion of velocity.

based on fuzzy logic, which can correct the longitudinal motion and the lateral motion synchronously. Compared with the existing methods, the proposed one has a better performance in dealing with flight constraints. Through synergistically correcting both longitudinal motion and lateral motion, the vehicle can realize more arduous mission. Moreover, in a correction cycle, the proposed method only requires a single trajectory prediction, which is favorable for on-board computation. The simulation results indicate that the proposed guidance law has a high precision and robustness.

Noting that the trajectory prediction is closely dependent on models of aerodynamic coefficients and atmospheric density, the prediction results can hardly be relied on when those models are not accurate. Therefore, the identification of aerodynamic coefficients and atmospheric density is very important. In this paper, the errors of those parameters are assumed to be constants. Therefore, the identification is not difficult to carry out. However, it is not so in real world scenarios. During further study, the error models based on fact are to be built and the error identification algorithm is to be studied.

Conflict of interest statement

There is no conflict of interest.

References

[1] J.C. Harpold, C.A. Graves, Shuttle entry guidance, J. Astronaut. Sci. 27 (3) (1979) 239–268.
[2] J.A. Leavitt, A. Saraf, D.T. Chen, K.D. Mease, Performance of evolved acceleration guidance logic for entry, in: AIAA Guidance, Navigation, and Control Conference and Exhibit, Monterey, California, USA, August, 2002.
[3] A. Saraf, J.A. Leavitt, D.T. Chen, K.D. Mease, Design and evaluation of an acceleration guidance algorithm for entry, in: AIAA Guidance, Navigation, and Control Conference and Exhibit, Austin, Texas, USA, August, 2003.
[4] Z.J. Shen, P. Lu, On-board generation of three-dimensional constrained entry trajectories, in: AIAA Guidance, Navigation, and Control Conference and Exhibit, Monterey, California, USA, August, 2002.
[5] J.P. Masciarelli, S. Rousseau, H. Fraysse, E. Perot, An analytic aerocapture guidance algorithm for the Mars sample return orbiter, in: Atmospheric Flight Mechanics Conference, Denver, Colorado, USA, August, 2000.
[6] J.F. Hamel, J.d. Lafontaine, Improvement to the analytical predictor–corrector guidance algorithm applied to Mars aerocapture, J. Guid. Control Dyn. 29 (4) (2006) 1019–1022.
[7] R.W. Powell, Numerical roll reversal predictor–corrector aerocapture and precision landing guidance algorithm for the Mars Surveyor Program 2001 missions, in: AIAA Atmospheric Flight Mechanics Conference and Exhibit, Boston, Massachusetts, USA, August 10–12, 1998.
[8] S.B. Xue, P. Lu, Constrained predictor–corrector entry guidance, J. Guid. Control Dyn. 33 (4) (2010) 1273–1281.
[9] H.F. Li, L. Xie, Reentry guidance law design for RLV based on predictor–corrector method, J. Beijing Univ. Aeronaut. Astronaut. 35 (11) (2009) 1344–1348.
[10] E.M. Yong, W.Q. Qian, K.F. He, An adaptive predictor–corrector reentry guidance based on self-definition way-points, Aerosp. Sci. Technol. 39 (2014) 211–221.
[11] M.L. Xu, L.H. Liu, Y. Yang, et al., Neural network based predictor–corrector entry guidance for high lifting vehicles, in: 62nd International Astronautical Congress, Cape Town, South Africa, October, 2011.
[12] P. Lu, Entry guidance: a unified method, J. Guid. Control Dyn. 37 (3) (2014) 713–728.
[13] P. Lu, Verification of a fully numerical entry guidance algorithm, J. Guid. Control Dyn. 40 (2) (2016) 230–247.
[14] Y. Xie, L.H. Liu, J. Liu, G.J. Tang, et al., Rapid generation of entry trajectories with waypoint and no-fly zone constraints, Acta Astronaut. 77 (2012) 167–181.